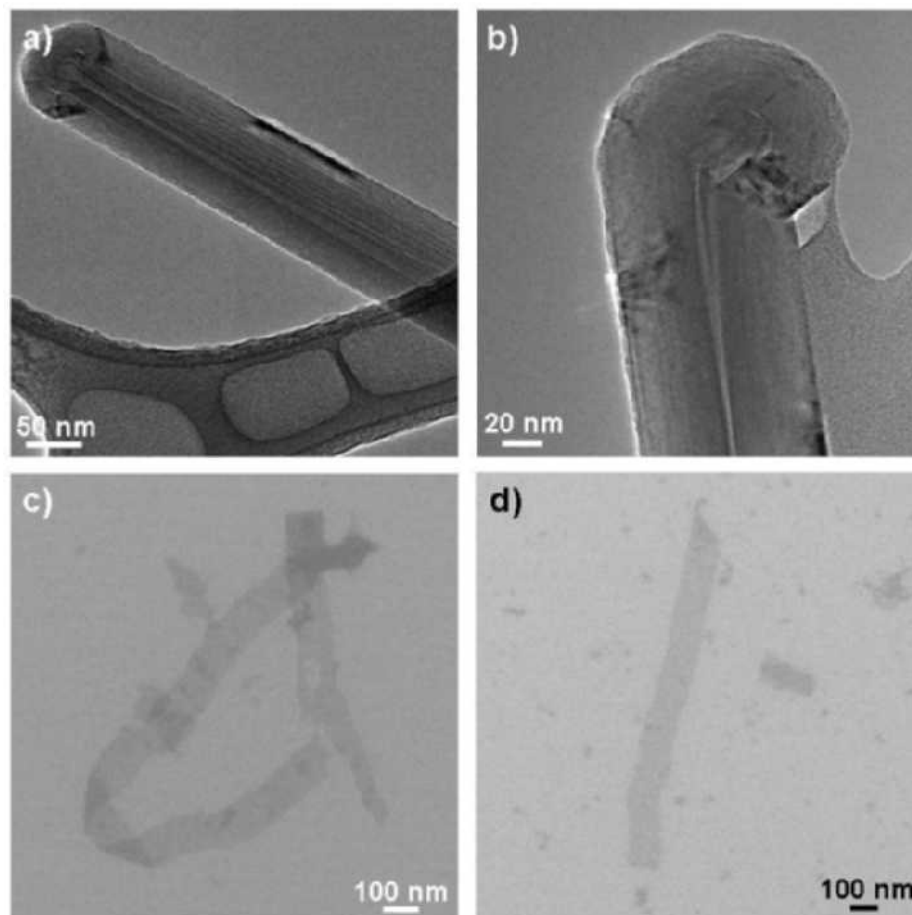**I. Additional analysis of Nanoribbons**
- TEM images of starting material MWCNTs
- TEM and SEM images of nanoribbons
- TGA weight loss curves and Raman spectroscopy of incremental oxidation
- XRD comparing oxidized nanoribbons to graphite oxide
- AFM image of nanoribbons after reduction with hydrazine
- Tabulated XPS data, Raman spectroscopy, and TGA weight loss curves before and after reduction

II. Analysis of Narrow Nanoribbons from SWCNTs
- TEM images
- AFM images
- UV-vis, IR, and XPS spectroscopy before and after reduction

I. Additional analysis of Nanoribbons

Figure S1. TEM analysis of Mitsui MWCNT starting material and additional SEM analysis of oxidized nanoribbons. a-b) TEM images of as-received MWCNTs. The average diameter is 40-80 nm with ~15-20 inner tube walls; the tips do not contain catalyst particles. c-d) SEM images of nanoribbons on a silicon surface.
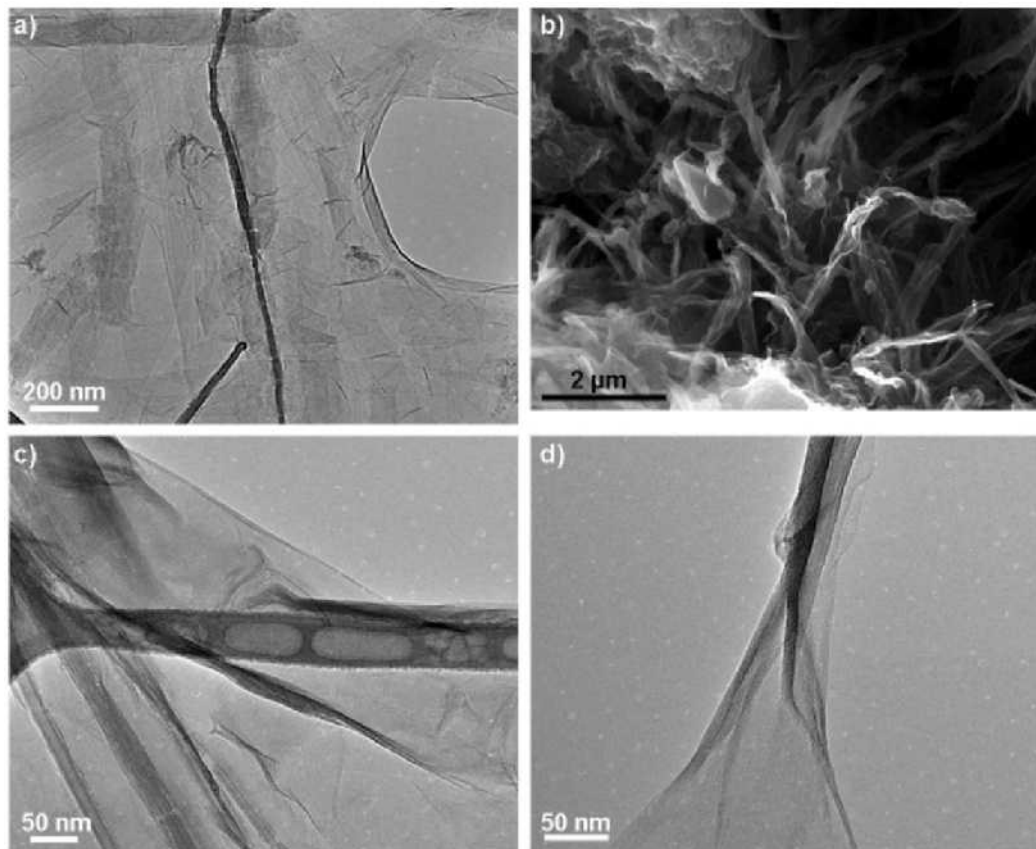
Figure S2. Additional TEM and SEM images of oxidized nanoribbons. a) An overview TEM image that highlights the high yield of the process. Very little MWCNT remains; the majority of the sample is overlaid ribbons with straight edges. b) SEM image of a bulk nanoribbon sample which also illustrates the high yield of the nanotube-free material. c) Wide nanoribbons; the bottom left portion shows some remaining MWCNT. d) A MWCNT in the process of unraveling.
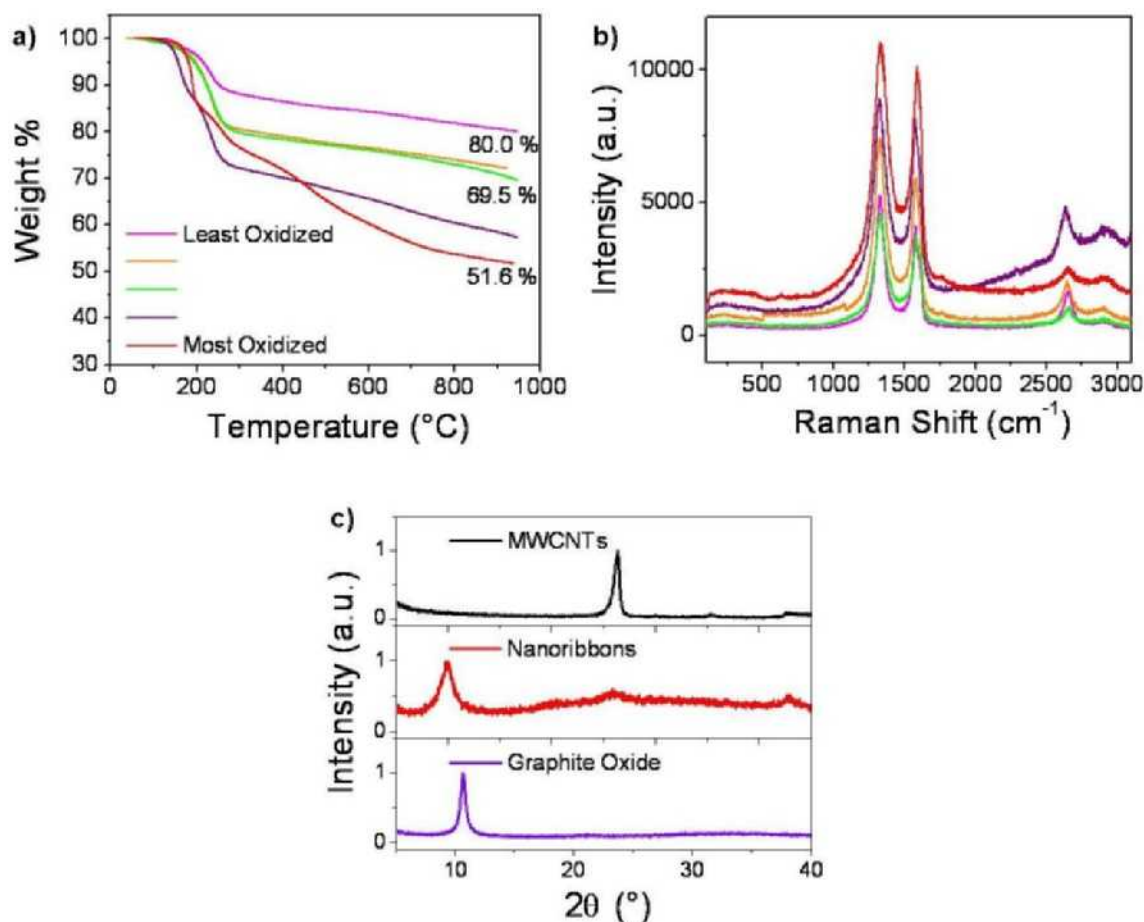
Figure S3. Analysis of incremental oxidation/nanoribbon formation from MWCNTs. Sample I represents a total of 100 wt % $KMnO_4$ used in the reaction, sample II is 200 wt % $KMnO_4$, etc. a) TGA weight loss curves of samples I-V; as the level of oxidation increases, the total amount of weight loss is increased. b) The Raman spectra of samples I-V; as the level of oxidation increases, the intensity and ratio of the D:G bands increases. c) XRD analysis showing the structure of the nanoribbons (red trace) in contrast to the MWCNT starting material (black trace) and the similarity in structure to graphite oxide (GO, violet trace prepared by the Hummers method[1] is shown with 2-theta ~10.6°). Comparing the XRD patterns of MWCNT and the nanoribbons, the (002) spacing shifted from 26° to 10° after oxidation, making it GO-like.
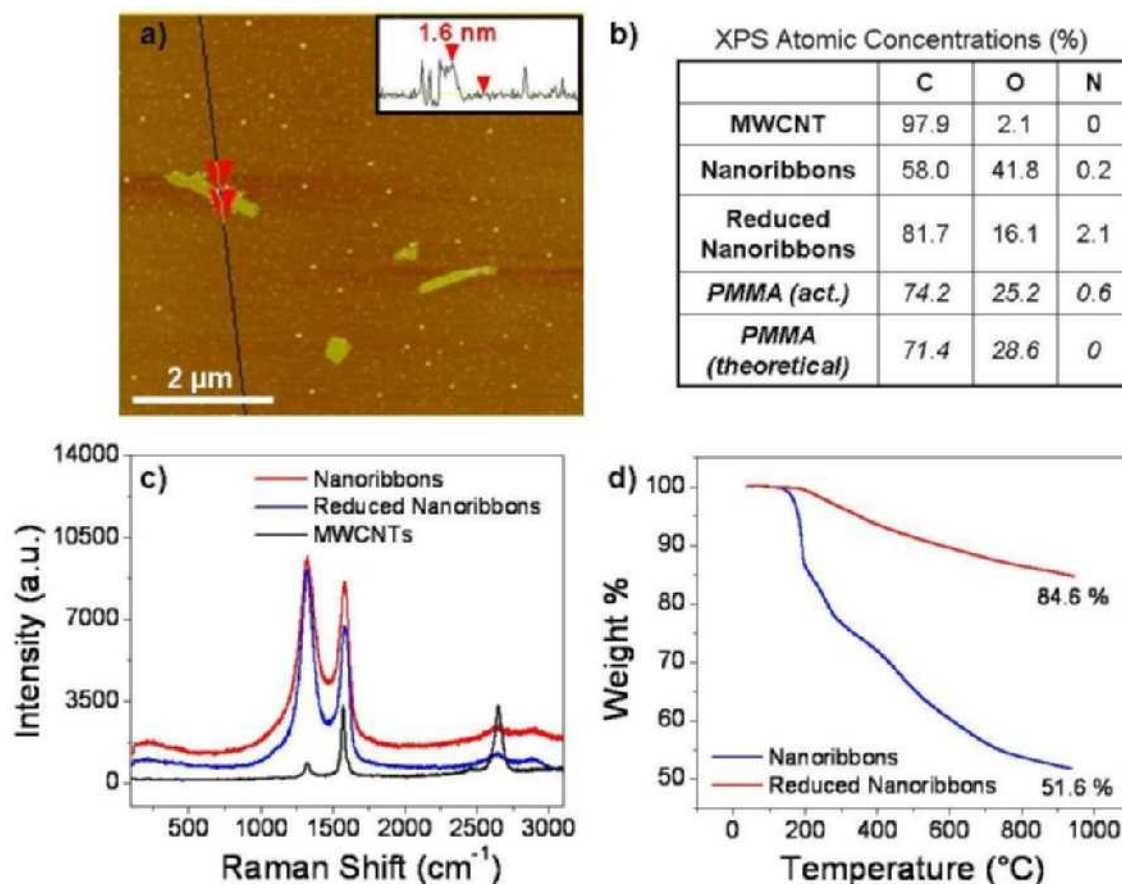
Figure S4. Comparison of oxidized and reduced nanoribbons derived from MWCNTs.

a) AFM image of nanoribbons post-reduction in the absence of surfactant. From the

height data, it is apparent that single layers of ribbons can be identified, but stacking

predominates without the surfactant. b) XPS determined compositions of oxidized and

reduced nanoribbons compared to the MWCNT starting material which corresponds to

the data shown in Figure 3b. A large loss of oxygen upon reduction is evident. A

poly(methyl methacrylate) (PMMA) standard was employed to determine the accuracy of

the measurement. The nitrogen content can be due to hydrazine adducts and physisorbed

N_2[2]. c) The Raman spectra of nanoribbons before (red) and after reduction (blue)

compared to the MWCNT starting material (black). The behavior is very similar to that

observed for GO and reduced GO[3] with a broadened G peak (1594 cm^{-1}) after oxidation along with the appearance of the D band at 1363 cm^{-1}. This indicates the reduction in size of the in-plane sp^2-carbon domains due to the oxidation. After reduction, both G and D bands are still prominent with an increased D:G intensity ratio compared to that of the oxidized form. This is expected and is caused by a decrease in the average size of the sp^2 domains upon reduction compared to the pristine material, but are more numerous in number than the GO sample[3]. d) TGA of nanoribbons before (red) and after reduction (blue) (10°C/min to 950°C under argon). Before reduction, the oxidized sample loses more total weight (49 %) than after reduction (15 %), a 33 % decrease. The oxidized sample experiences a sharp drop at ~200°C due to dehydration and possible decarboxylation of the oxygen-containing functional groups yielding CO$_x$[4,5]. The absence of such groups in the post-reduction sample increases the thermal stability and results in the weight loss curve to be more gradual[3].

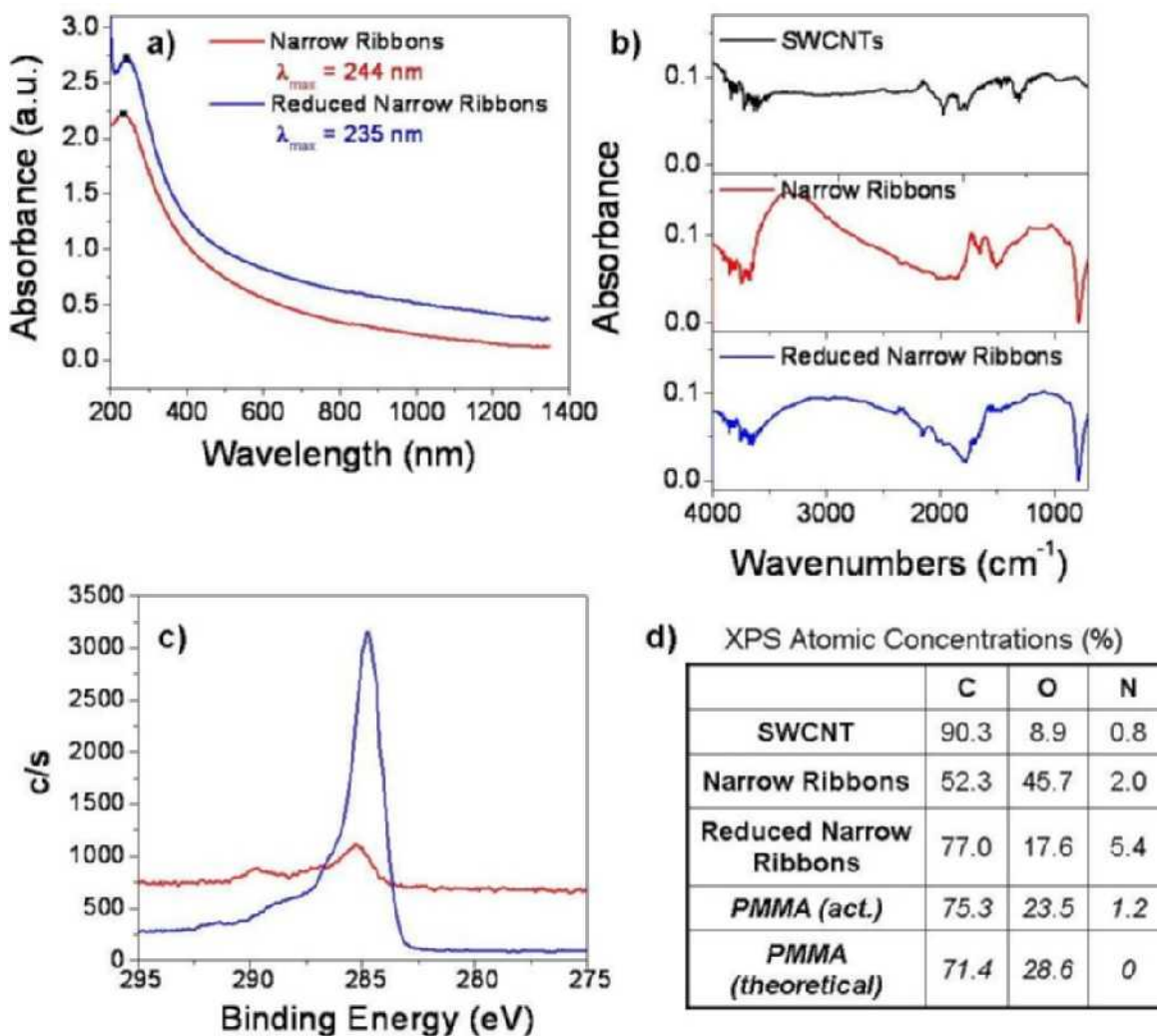## II. Analysis of Narrow Nanoribbons from SWCNTs

TEM and AFM images of the product obtained from KMnO$_4$ treatment of SWCNTs yielded similar results as those from MWCNTs and appear to produce "narrow" nanoribbons. Compared to the starting SWCNTs (Fig. S5a) with their 1-2 nm heights as individuals and to 3-5 nm in heights when bundled, the resulting nanoribbon structures appear to be flatter, less bundled, and have larger widths. The narrow nanoribbons from SWCNTs appear more twisted and aggregated than the MWCNT-derived samples. The SWCNTs used were produced via the HiPco process[6] (batch number 187.4) by the Carbon Nanotechnology Laboratory at Rice University. The SWCNTs were purified before use to lower the catalyst content[7]. The procedure for

preparation of narrow nanoribbons from SWCNTs is the same as that from MWCNTs with the following modifications: 25 % by volume fuming sulfuric acid is used to suspend purified SWCNTs prior to oxidation. In addition, after the $KMnO_4$ (500 wt %) has stirred in the reaction mixture at room temperature for 1 h, the reaction is typically complete after heating at 55 °C for an additional 45 min.
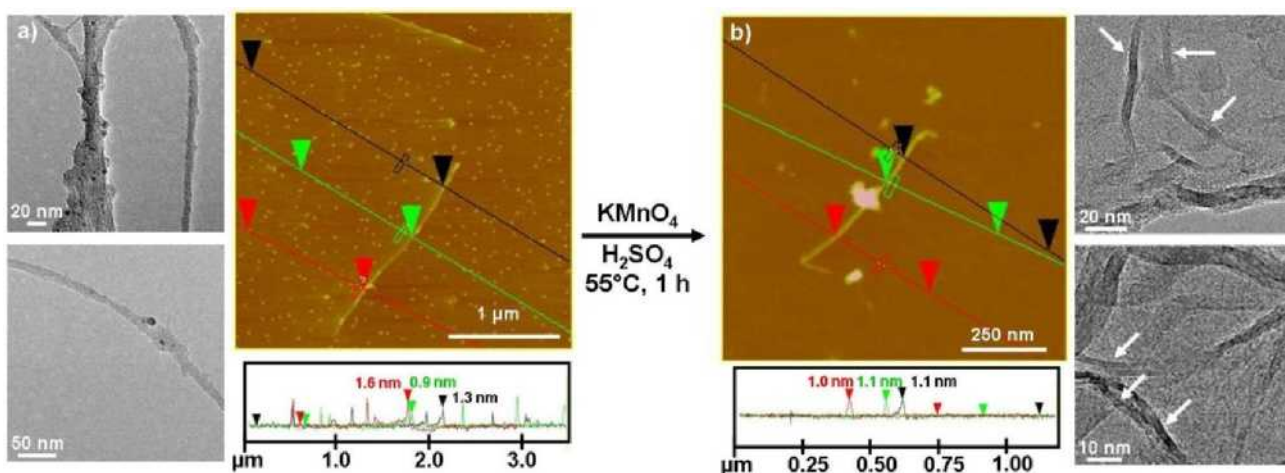
Figure S5.   TEM and AFM images depicting the transformation of SWCNTs into oxidized narrow nanoribbons. a) Starting material SWCNTs produced via the HiPco process. The TEM images (left) consist of bundled purified SWCNT structures that are 5-10 nm in diameter with residual Fe catalyst particles. The SWCNT sample used in the AFM image (right) was taken from the same batch of SWCNTs that had been suspended as individuals in SDS surfactant (via previously reported procedures[8]) so that accurate height data could be obtained on single tubes. The average height of the single SWCNT shown is ~1.3 nm. The dot structures are traces of surfactant; most of the surfactant was removed with isopropanol during spin-coating of the AFM sample. b) Resulting material after treatment with $KMnO_4$ in sulfuric acid at 55°C for 45 min. The AFM image (left)

with a decreased average height (~1 nm). TEM images (right) reveal that the ribbon structures remain closely associated to one another, intertwined and mostly stacked in a "bowl of noodles" arrangement. Flat narrow nanoribbons, stacked and unstacked, with diameters of ~3-5 nm (noted by white arrows), can be identified.

Figure S6. Characterization of the oxidized and reduced narrow nanoribbons derived from SWCNTs. a) Changes in the UV spectrum of an aqueous solution of narrow nanoribbons (red) upon treatment with N_2H_2 (blue). Bathochromic shift of the absorption

maximum and significant hyperchromicity in the absorption across the entire spectral range (intensities are to-scale) are evident, but less pronounced than for the MWCNT-derived nanoribbons. b) ATR-IR of narrow nanoribbons before (red) and after reduction (blue) compared to SWCNT starting material. The oxidized ribbons retain water as demonstrated in the broad –OH absorption. After reduction, water retention and the amount of functionality is decreased, but not eliminated as observed for the MWCNT-derived ribbons due to much higher proportion of carboxylic acids to total carbon atoms contained on the edges of the narrow nanoribbons as compared to the wider nanoribbons. c) Superimposed XPS C1s spectra of the oxidized (red) and the reduced nanoribbons (blue). The signals at 286 eV and 287 eV correspond to C-O and C=O, respectively. The shoulder at 289 eV is assigned to carboxy groups. After reduction, the 286 eV and 287 eV peaks become much smaller demonstrating significant deoxygenation of the nanoribbons by N_2H_4. As reported for CCG, the most dominant peak after chemical reduction is the C-C peak (284.8 eV)[9]. d) XPS-determined atomic compositions of oxidized and reduced narrow nanoribbons compared to the SWCNT starting material. Significant oxygen loss is seen upon reduction. A poly(methyl methacrylate) (PMMA) standard was employed to determine the accuracy of the measurement. The nitrogen content can be due to hydrazine adducts and physisorbed N_2[2].

References for the Supplementary Information

1.   Hummers, W. S., Jr. & Offeman, R. E. Preparation of graphitic oxide. *J. Am. Chem. Soc.* **80**, 1339 (1958).

2.   Kang, E. T., Neoh, K. G. & Tan, K. L. X-ray photoelectron spectroscopic studies of electroactive polymers. *Adv. Polym. Sci.* **106**, 135-90 (1993).

3.   Stankovich, S. *et al.* Synthesis of graphene-based nanosheets via chemical reduction of exfoliated graphite oxide. *Carbon* **45**, 1558-1565 (2007).

4.   Hung, C.-c. & Corbin, J. Synthesis and thermal stability of graphite-oxide-like materials. *Carbon* **37**, 701-705 (1999).

5.   Lerf, A., He, H., Forster, M. & Klinowski, J. Structure of Graphite Oxide Revisited. *J. Phys. Chem. B* **102**, 4477-4482 (1998).

6.   Nikolaev, P. *et al.* Gas-phase catalytic growth of single-walled carbon nanotubes from carbon monoxide. *Chem. Phys. Lett.* **313**, 91-97 (1999).

7.   Chiang, I. W. *et al.* Purification and Characterization of Single-Wall Carbon Nanotubes (SWNTs) Obtained from the Gas-Phase Decomposition of CO (HiPco Process). *J. Phys. Chem. B* **105**, 8297-8301 (2001).

8.   O'Connell, M. J. *et al.* Band gap fluorescence from individual single-walled carbon nanotubes. *Science* **297**, 593-596 (2002).

9.   Stankovich, S. *et al.* Stable aqueous dispersions of graphitic nanoplatelets via the reduction of exfoliated graphite oxide in the presence of poly(sodium 4-styrenesulfonate). *J. Mater. Chem.* **16**, 155-158 (2006).